

# The broad-band X-ray spectrum of the blazar PKS B1830–211 by *Chandra* and *INTEGRAL*

A. De Rosa<sup>1</sup>, L. Piro<sup>1</sup>, A. Tramacere<sup>2</sup>, E. Massaro<sup>1,2</sup>, R. Walter<sup>3</sup>, L. Bassani<sup>4</sup>, A. Malizia<sup>4</sup>, A.J. Bird<sup>5</sup>, and  
A.J. Dean<sup>5</sup>

<sup>1</sup> IASF - Sezione di Roma, INAF, via del Fosso del Cavaliere, I-00113 Roma, Italy

<sup>2</sup> Dipartimento di Fisica, Università La Sapienza, Piazzale A. Moro 2, I-00185 Roma, Italy

<sup>3</sup> Geneva Observatory, INTEGRAL Science Data Centre, Chemin d'Ecogia 16, 1291 Versoix, Switzerland

<sup>4</sup> IASF - Sezione di Bologna, INAF, via P. Gobetti 101, I-40129 Bologna, Italy

<sup>5</sup> School of Physics and Astronomy, University of Southampton, Highfield, Southampton, SO17 1BJ, UK

Received ....; accepted ....

**Abstract.** In this paper we present a broad-band study of the X-ray emission of the blazar PKS 1830–211 based on *Chandra* and *INTEGRAL* observations. Notwithstanding the high redshift ( $z=2.507$ ), it is a bright X-ray source ( $F(2-10\text{ keV}) \simeq 10^{-11}\text{ erg cm}^{-2}\text{s}^{-1}$ ), due to gravitational lensing by an intervening galaxy at  $z=0.89$ . Previous X-ray observations attribute the observed absorption at  $E < 2\text{ keV}$  to the lensing galaxy. Our analysis, although not in contrast with this hypothesis, suggests also the possibility of an intrinsic (ionized) absorption, taking place at the front side of the jet. This scenario is also supported by some evidence, in the same data, of a feature observed at  $2.15\text{ keV}$  which can be interpreted as a blueshifted iron line ( $v/c \simeq 0.18$ ). The SED of PKS 1830–211 can be well modelled by combining a Synchrotron Self-Compton component and an external source of photons to be scattered up to  $\gamma$ -ray energies by relativistic electrons moving outward in the jet. The main source of low energy photons is a dust torus at the temperature of  $10^3\text{ K}$  as expected in MeV blazars.

**Key words.** radiation mechanisms: non-thermal - galaxies: active - X-rays: galaxies: individual: PKS B1830–211

## 1. Introduction

PKS B1830–211 is a high redshift blazar ( $z = 2.507$ , Lidman et al. 1999) gravitationally lensed by an intervening galaxy at  $z = 0.89$ . Its radio image shows two compact components separated by about  $1''$  and believed to arise from the core of the source (hereafter North-East NE and South-West SW components), plus a ringlike extended structure arising from the jet (Wiklind & Combes 1996), connecting the compact components (Nair et al. 1993, Pramesh Rao & Subrahmanyan 1988). In the radio band the source shows strong variability (Lovell et al. 1998) and has a flat spectrum. It was also observed in the infrared (Lidman et al. 1999), in the X-rays (Mathur & Nair 1997, Oshima et al. 2001) and in the  $\gamma$ -rays (Mattox et al. 1997, Bassani et al. 2004).

*ROSAT* data showed that the X-ray spectrum is best represented by a power law absorbed at the redshift of the lens galaxy by a column density  $N_H = (3.5 \pm 0.5) \times 10^{22}\text{ cm}^{-2}$ ; no additional absorption component was required, suggesting that both lensed images are covered by the same absorber (Mathur & Nair 1997).

On the contrary, *ASCA* data showed that the spectrum is consistent with two absorption components having different column densities:  $N_H^{\text{low}} < 1.5 \times 10^{22}\text{ cm}^{-2}$  and  $N_H^{\text{high}} = (7.5 \pm_{-0.9}^{+0.8}) \times 10^{22}\text{ cm}^{-2}$  (Oshima et al. 2001), explained by the authors with the view that the low- and high-absorbing component correspond to the NE and SW lensed images, respectively. The ratio of the two magnification factors was  $0.21^{+0.07}_{-0.08}$ , smaller than the value found at radio wavelengths which was  $1.55 \pm 0.02$  (Lovell et al. 1998). In this paper we investigate the broad-band X-ray spectrum of PKS 1830–211 observed by *Chandra* and *INTEGRAL*. In section 2 we describe the observations while data analysis is presented in Section 3. In section 4 the nature of the complex absorber is discussed, while in Section 5 the SED of PKS 1830–211 is derived and a possible emission model is presented. We summarize our results and conclusions in Section 6.

## 2. Observations and data reduction

### 2.1. INTEGRAL

PKS1830-211 is one of the AGNs detected by *INTEGRAL* in the Galactic Center region (Bassani et

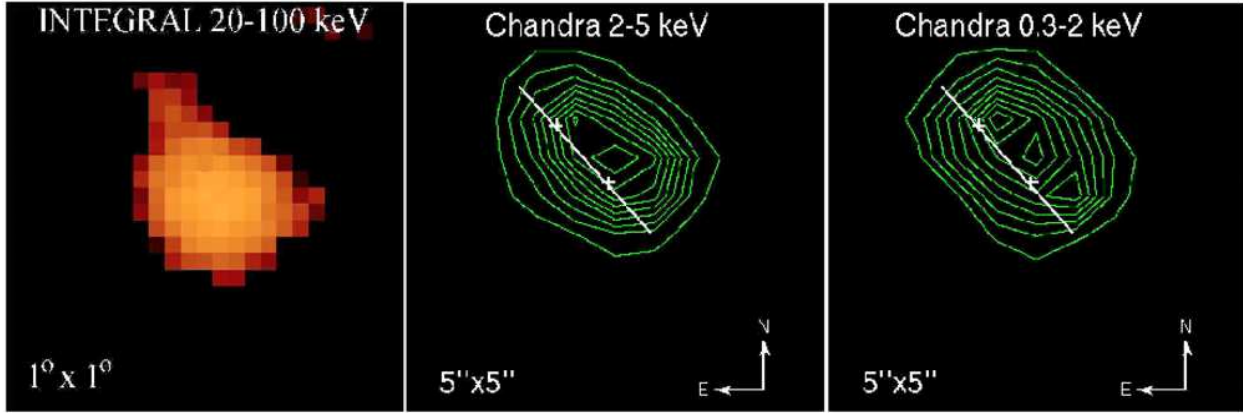


**Fig. 1.** X-ray images of PKS 1830–211. The *INTEGRAL* image is shown in the left panel, its extension is compatible with the PSF of ISGRI. In the middle and right panel we show the *Chandra* contour levels in two different energy range together with the position of the NE and SW lobes from radio observations (Pramesh Rao & Subrahmanyan 1988). The two main components of the lensing are distinguished in *Chandra* images.

al. 2004). It has been reported as an *ISGRI* source by Bird et al. (2004) and Revnivtsev et al. (2004) and at a redshift of 2.507 it is the farthest object so far detected by *INTEGRAL*. The observational data reported here refer to the first *IBIS* survey which consists of several pointings carried out between 2003 February 28 to October 10. The total on source exposure is 714 ksec, providing a detection at  $\sim 14\sigma$  confidence level. The mean counting rate is  $0.29 \pm 0.03$  counts  $s^{-1}$  both in the 20–40 and 40–100 keV band, a clear indication of a hard spectrum. These count rates correspond to a flux of roughly 3 (2.4) and 4 (3.9) mCrab ( $10^{-11}$  erg  $cm^{-2}$   $s^{-1}$ ) in the two bands, respectively. *ISGRI* images for

each available pointing were generated in narrow energy bands using the ISDC offline scientific analysis software OSA version 3.0 (Goldwurm et al. 2003), including background uniformity corrections (Terrier et al. 2003). Source ghosts have been removed from each image using a catalogue built iteratively and containing at end all sources detected. The individual images were then combined to produce a mosaic of the region of interest in broader bands to enhance the detection significance using the system described in details by Bird et al. (2004).

The combined 20–100 keV image of the source is shown in the left panel in Figure 1. The *ISGRI* image is point-like, the extension is compatible with the PSF of the instrument.

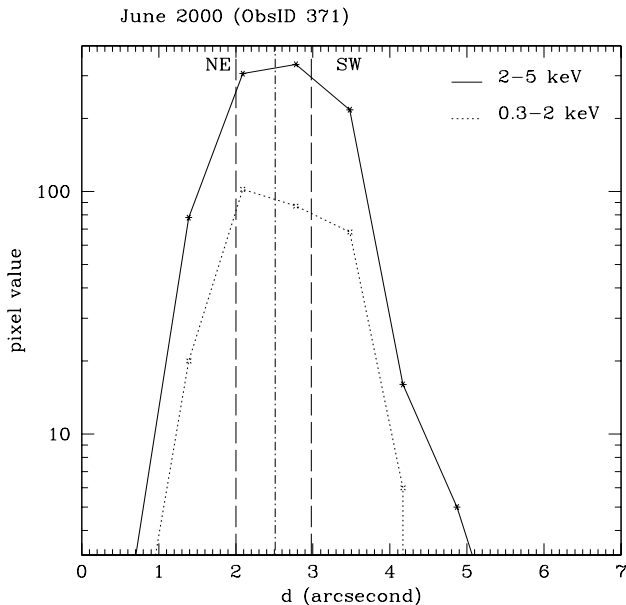


**Fig. 2.** X-ray intensity profiles along the major axis of the ellipse in the case of the *Chandra* observation in 2000 June.

## 2.2. Chandra

*Chandra* observations of PKS B1830–211 were performed on two occasions, one year apart in 2000 June 26–27 and 2001 June 25, for a total exposure of about 50 ks. The source did not show evidence of variability between the two pointings. The good spatial resolution allow us to observe the two lensed images, with an angular distance of the order of the *Chandra* resolution limit ( $\sim 1''$ ). In Figure 1 we show the ACIS contour levels extracted in two separate energy ranges 0.3–2 keV (right panel) and 2–5 keV (middle panel). In the figure we indicate also the position of the NE and SW component taken from radio observation (Pramesh Rao & Subrahmanyan 1988). The offset between radio and X-rays image is less than  $1''$ . There is evidence for an ellipsed shape in both images, as showed by the plotted contours, and the two main components of the lensing effect are visible. In Figure 2 we plot the X-ray intensity profiles along the major axis of the ellipse which shows that it is significantly larger than the ACIS PSF. The ACIS PSF is very sharply peaked on-axis, with

a FWHM less than half an arcsec<sup>1</sup>. The ratio between the counts from the NE and SW components is about 1.5 in both 0.3–2 keV and 2–5 keV energy range similar to the value observed at radio frequencies. This result indicates that the absorbing gas column densities of the two components cannot be very different, contrary the findings of Courbin et al. (2002) in the optical and near-IR, where the SW component seems to be much weaker than the NE one.

### 3. Spectral analysis and results

Spectral analysis has been performed fitting the data of both *Chandra* observations combined together, in fact fitting them separately does not provide evidence for a significant difference. We first apply a simple power-law absorbed by Galactic gas ( $N_H^{Gal} = 2.6 \times 10^{21} \text{ cm}^{-2}$ , Stark et al. 1992) in the whole range 0.5–8 keV and obtain a poor fit with  $\chi^2/\text{dof}=725/459$ . A better result is found fitting the data at energies higher than 2 keV, where the absorption is not relevant. In this case the above model gives a  $\chi^2/\text{dof}=389/377$  with a photon index  $\Gamma=1.02\pm0.05$  and an estimated flux  $F_{2-10} \simeq 10^{-11} \text{ erg cm}^{-2} \text{ s}^{-1}$ . However, the data to model ratio in the energy range 2–8 keV shows clear systematic residuals below 5 keV in the source frame (Figure 3). *INTEGRAL* spectrum in the hard X-ray energy range 20–80 keV is also well reproduced by this flat power-law model, confirming that the broad-band spectrum remains remarkably flat up to 80 keV. This will be discussed in more detail in the next Section.

### 4. The nature of the absorption

Spectral flattening at energies less than 2 keV has been found in radio-loud quasars having a redshift up to 4.4, using *ASCA* and *XMM-Newton* data (Fiore et al. 1998, Reeves & Turner 2000, Worsley et al. 2004, Yuan et al. 2003 and references therein). Absorption has been suggested as the likely explanation for this flattening but the data collected up to now do not allow one to distinguish between an intrinsic absorber at the source redshift or an absorbing system along the line of sight. However, the UV-optical extinction observed in most of these objects, is inconsistent with the high column density required to produce the flattening observed in X-rays. It was suggested that this gas could be ionized (Fabian et al. 2001), i.e. a *warm absorber* similar to that present in Seyfert 1 galaxies. Another possibility is that of an intrinsic low energy cut-off in the electron spectrum as proposed for other similar objects (Celotti & Fabian 1993, Sikora et al. 1997).

First, we attempted to reproduce the low-energy spectral break with a cold absorber (in addition to the Galactic one) at the redshift of the lens galaxy ( $z=0.89$ ) as proposed by previous *ROSAT* (Mathur & Nair 1997) and *ASCA* (Oshima et al. 2001) observations. The best fit values are reported in the first line of Table 1. *Chandra*

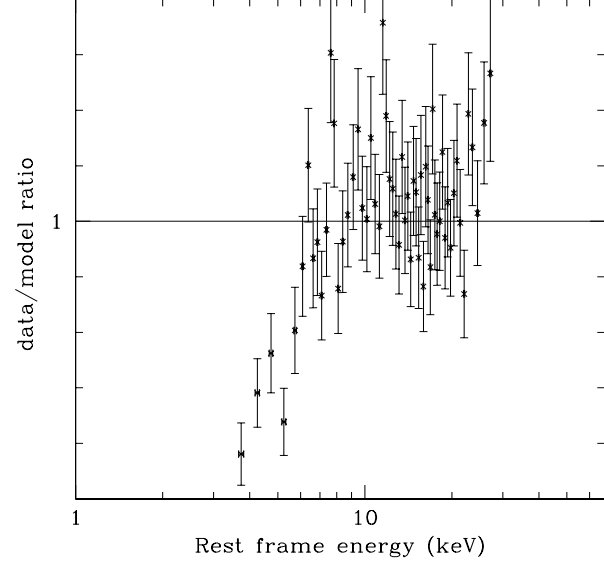


**Fig. 3.** Ratio of *Chandra* data of both observations to a  $\Gamma = 1.02$  simple power-law (including Galactic absorption  $N_H^{Gal} = 2.6 \times 10^{21} \text{ cm}^{-2}$  and fitted over the 2–8 keV range) in the source frame. Note the large residuals at energies below 5 keV.

data of both observations are well fitted with a single flat power-law, with photon index  $\Gamma=1.09\pm0.05$ , absorbed by a cold gas with  $N_H \simeq 2 \times 10^{22} \text{ cm}^{-2}$  at  $z=0.89$  ( $\chi^2/\text{dof}=482/458$ ). Data and the folded model are shown in Figure 4 (left panel). *INTEGRAL* data, taken one year after *Chandra* observation, are also well reproduced by this continuum. The constant of cross-calibration *Chandra*/*INTEGRAL* was free to vary during the fit and was found to be  $C=0.57\pm0.13$ . The broad-band spectrum of PKS 1830–211 is shown in Figure 5, and the best fit values are reported in the last line of Table 1.

We also test the possibility that the absorbing gas is intrinsic to the source, by fitting *Chandra* data with a warm absorber model. Best fit values are reported in the second line of Table 1. The fit is good ( $\chi^2/\text{dof}=517/457$ ) even if not better with respect to that of a cold gas at  $z=0.89$ . This result suggests the presence of a mildly ionized gas with the column density  $N_H \simeq 10^{23} \text{ cm}^{-2}$ , and an upper limit to the ionization parameter  $\xi = L_{2-10}/nR^2 < 100 \text{ erg cm s}^{-1}$ , where  $L_{2-10}$  is the inferred isotropic luminosity in the 2–10 keV rest frame of the blazar while  $n$  and  $R$  are the absorber density and the distance from the source, respectively.

*Chandra* data show some evidence ( $\approx 3\sigma$ ) in each observations of an emission feature around 2.15 keV with an intensity of  $2 \times 10^{-5} \text{ ph cm}^{-2} \text{ s}^{-1}$  and an equivalent width of about 50 eV (see right panel in Figure 4). The line is not resolved in the ACIS-S, setting the intrinsic width to be  $< 50 \text{ eV}$ . *Chandra* -HETG spectra are consistent with ACIS data, and set a lower limit on the intrinsic width to

<sup>1</sup> See *The Chandra Proposers Observatory Guide* (<http://asc.harvard.edu/proposer/POG/html/MPOG.html>)

**Table 1.** Results of the spectral fits of *Chandra* and *INTEGRAL* observations. Confidence ranges are 90 per cent for one parameter.

	$\Gamma$	${}^1N_{H,z}/{}^1N_{H,ion}$	${}^2\xi$	${}^3F_{2-8keV}^{una}$	${}^3F_{2-80keV}^{una}$	${}^3F_{0.5-8keV}^{una}$	$\chi^2/\text{dof}$
0.5-8keV	$1.09^{+0.05}_{-0.05}$	$1.93^{+0.27}_{-0.26}$	-	0.78	8.6	1	482/458
0.5-8keV	$1.06^{+0.05}_{-0.05}$	$9.5^{+4.4}_{-2.1}$	$< 100$	0.78	9.1	1	517/457
0.5-80keV	$1.09^{+0.05}_{-0.05}$	$1.94^{+0.28}_{-0.25}$	-	0.78	8.5	1	485/462

Note:  ${}^1N_{H,z}$  is the column density at redshift of the lens galaxy  $z=0.89$ ,  $N_{H,ion}$  is the column density of the warm gas at redshift of the source  $z=2.51$ , both are in  $10^{22} \text{ cm}^{-2}$ ;  ${}^2\xi$  in  $\text{erg cm s}^{-1}$ ;  ${}^3F$  in  $10^{-11} \text{ erg cm}^{-2} \text{ s}^{-1}$

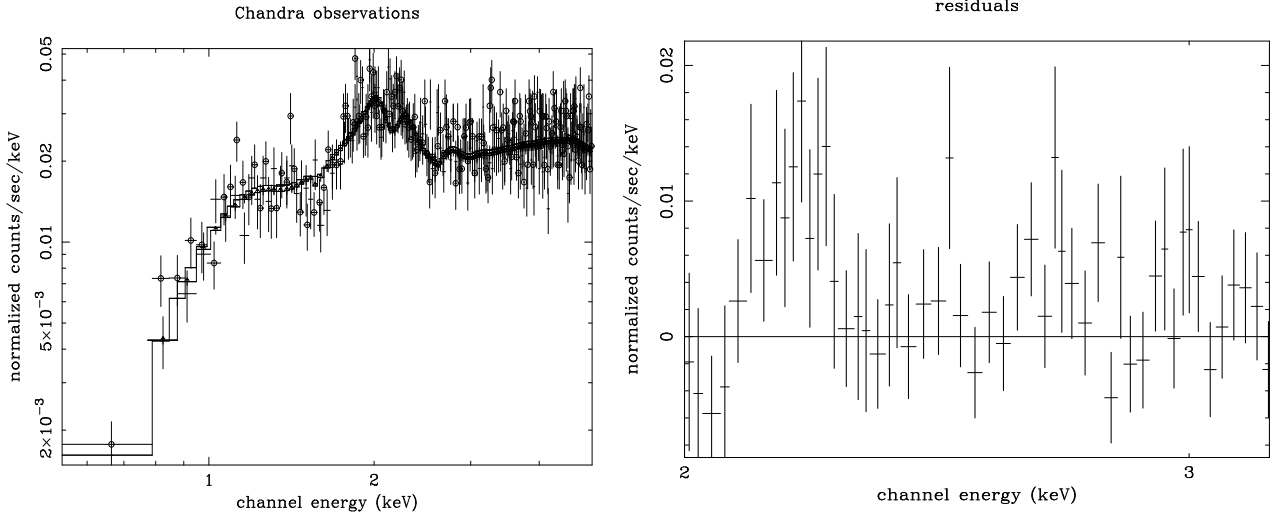


**Fig. 4.** In the left panel we show the *Chandra* spectra of both 2000 and 2001 observations with the folded model characterized by a power-law absorbed by a cold gas at the redshift of the lens galaxy. The data taken in 2001 are plotted with a circle. A zoom of the residuals in the line feature region, from *Chandra* ACIS-S, is shown in the right panel.

be 10 eV. It is important to note that the residuals around the line are of the order of few tens of per cent, while the instrumental systematic effects at this energy are of the order of few per cent. The energy of the line at the redshift of PKS 1830–211 is 7.54 keV – thus suggesting an association with a blueshifted iron line. This feature could be produced in the ambient matter around the source. If the line is due to neutral iron, the implied velocity for the gas has to be  $v \simeq 0.18c$ . It is interesting to note that if the warm gas with a column density of  $\sim 10^{23} \text{ cm}^{-2}$  covers a solid angle of  $2\pi$  to the source, it should produce a line with  $\text{EW} \simeq 50 \text{ eV}$ , consistent with that detected in *Chandra* spectrum.

## 5. The Spectral Energy Distribution

We then used our spectral results and other data available in the literature to derive the SED of PKS 1830–211 shown in Figure 6. Of course, it is not based on simultaneous observations and therefore must be considered

an indicative picture of the emission properties of this source.  $\gamma$ -ray data are from the EGRET public archive (<ftp://coss.gsfc.nasa.gov/compton/data/egret/>) and indicate a quite steep spectrum with a photon index of  $2.58 \pm 0.13$ . IR and optical points have been derived from the photometric data of the NE component given by Courbin et al. (2002), multiplied by 2 to take into account the obscured contribution from the SW component. These data have been corrected for an equivalent galactic absorption  $A_V=6.0$ , slightly smaller than the  $N_H$  value expected from the *Chandra* data best fit. The galactic contribution to  $A_V$ , estimated from  $E(B-V)=0.46$  (Schlegel et al. 1998), is 1.44 ( $R = 3.1$ ), whereas the additional absorption from the lens galaxy is of the order of 4 mag (Winn et al. 2002). We recall that optical images show that the SW component is much higher absorbed with a differential reddening of  $E(B-V) \simeq 2.75$  (Courbin et al. 2002).

A further problem is the magnification factor of the flux due to the gravitational lens. Following the numerical calculations for the lens modelling by Nair et al. (1993) we assumed the magnification factor for the summed flux of both components to be equal to 10 (see also Mathur & Nair 1997). A lower factor, of course, would increase the intrinsic luminosity of PKS 1830–211.

We then tried to apply some emission models to reproduce the SED according to the largely accepted scenarios used for high luminosity Blazars. First, we used a single zone homogeneous Synchrotron-Self Compton (SSC) model, but it failed to reproduce at the same time the radio-optical bump and the X and  $\gamma$ -ray bump. The SSC model contains a number of free parameters whose values were chosen on the basis of the current blazar physics: we assumed then the beaming factor  $\delta=16$  and a mean magnetic field  $B=0.8$  G, comparable to those considered for 3C 279 (Hartman et al. 2001). The very high beamed luminosity,  $\sim 4 \times 10^{48}$  erg s $^{-1}$  after the correction for the lens magnification, requires a population of emitting electrons confined inside a volume of about  $10^{53}$  cm $^3$  and an electron density of 850 cm $^{-3}$ . The steady electron energy distribution is a broken power law with the break at the Lorentz factor  $\gamma_b \simeq 70$ , obtained equating the electron cooling time to the crossing time through the emitting volume. The two spectral indices are  $p_1 = 1.80$  for  $\gamma < \gamma_b$  and  $p_2 = 2.80$  above the break. These values were chosen to match together X and  $\gamma$ -ray data are their difference is that expected from radiative cooling. The maximum Lorentz factor is 2500, suited to reproduce the decline of synchrotron spectrum at optical-UV.

The resulting SED is plotted in Figure 6. Note that the synchrotron self absorption frequency (defined by unitary optical depth) is around  $3 \times 10^{11}$  Hz in the observer's frame and therefore there is no way to account for the emission in the GHz band. The same problem, found for other blazars like 3C 279 (Hartman et al. 2001) and PKS 1127–145 (Blazejowski et al. 2004), can be solved assuming a multi-component model in which the radio emission comes from an outer region where the magnetic field is lower. Notice, however, that this SSC model gives hard X and  $\gamma$ -ray luminosities lower than the observed values by more than an order of magnitude.

External Radiation Compton (ERC) models consider that the main sources of seed photons are the accretion disk around the massive black hole, the broad line region and, at larger distances, the dust torus. UV photons from the disk are seen deboosted by the relativistic electrons moving outward in the jet from behind and their contribution is small. When computing ERC considering only photons originating in an accretion disk with a luminosity of  $4 \times 10^{48}$  erg s $^{-1}$  and a multitemperature spectrum ( $T_{max} = 3.5 \times 10^5$  K, Shakura and Sunyaev 1973) we obtain a Compton bump much lower than the data. Moreover, photons scattered by the BLR give another relevant but not a sufficient contribution to IC bump. An increase of  $\gamma_b$  would move the peak frequency above  $10^{23}$

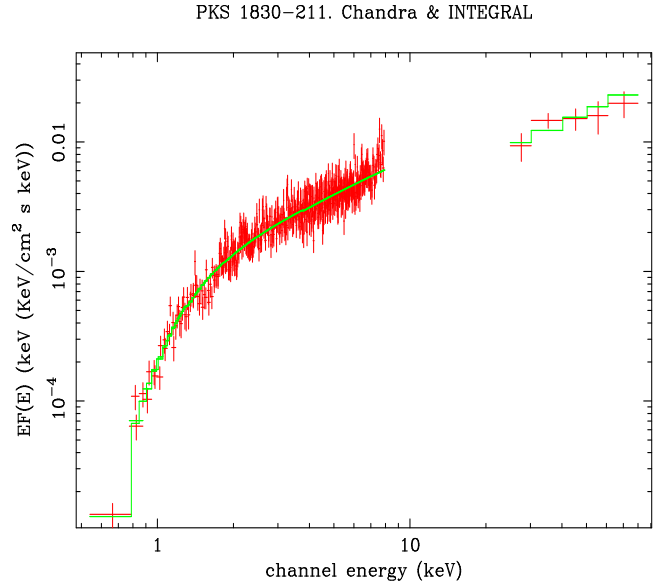


**Fig. 5.** Broad-band spectra of PKS 1830–211 from *Chandra* and *INTEGRAL*. The observations have been performed about one year apart. The data are reproduced with a power-law with  $\Gamma \simeq 1.1$  absorbed at  $z=0.89$  by  $N_H \simeq 2 \times 10^{22}$  cm $^{-2}$  (in addition to the Galactic absorption at  $z=0$ ).

Hz which is in conflict with the steep spectrum observed in the EGRET range.

More suitable are photons produced by matter at a distance of a few pc and illuminated by the disk, like the IR emission from a dusty torus at a temperature of  $10^3$  K as expected in similar sources (Sikora et al. 2002, see next section). Given the geometry of the jet-disk ambient, and the positioning of the emitting volume at a distance of  $\sim 10^{19}$  cm from the accretion disk, we find that the comoving energy density of the IR external photon field from the dust torus overwhelms the other soft field at least by an order of magnitude. The resulting IC bump is able to reproduce both the X and  $\gamma$ -ray continuum. We recall, however, that the latter data are not a strong constraint because of source variability, which in this range is at least a factor of 4, as indicated from the 3EG catalogue (Hartman et al. 1999).

## 6. Discussion

It is interesting to compare the properties of this distant and lensed blazar with those of other sources of the same class. The SED of Figure 6 shows that the largest energy output is in the prominent IC bump. A relevant finding of our analysis is that the X-ray spectrum of PKS 1830–211 is remarkably flat up to energies of  $\sim 80$  keV, while the spectrum above  $\sim 100$  MeV is much steeper. The difference between these two spectral indices is around 1.5. The peak frequency, however, is not well constrained by the data: in the model described in the previous section it lies around

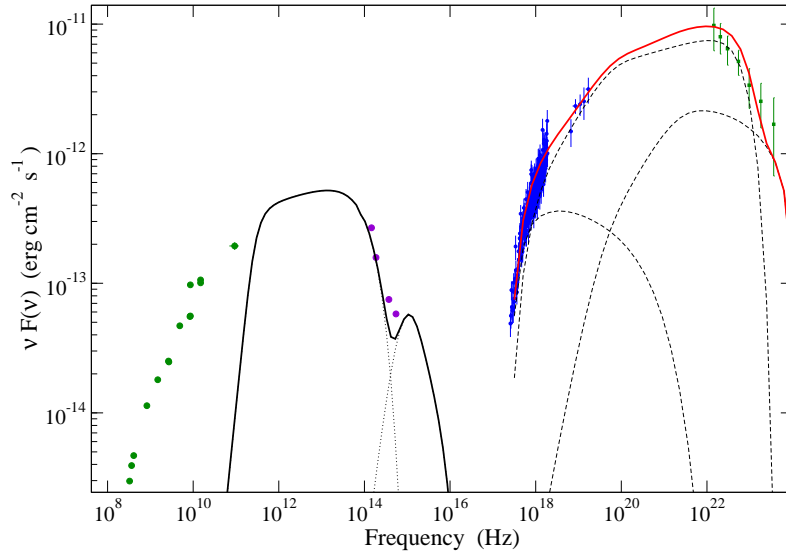


**Fig. 6.** The Spectral Energy Distributions of PKS 1830–211 in the observers’ frame derived from our results and other published data. Radio measurements are from Pramesh Rao & Subrahmanyan (1988), IR and optical data from Courbin et al. (2002) and  $\gamma$ -ray data from the EGRET public data archive. Solid lines represent the SED as the sum of various emission contributions computed with the parameters given in the text; dotted lines are the individual low energy contributions: synchrotron emission and accretion disk; dashed line are high energy spectra of SSC (lower bump) and ERC components.

$10^{22}$  Hz, however it could be lower, in the MeV range, for a different electron spectrum. PKS 1830–211 can be considered a member of the small subclass of “MeV blazars” discovered by COMPTEL (Bloemen et al. 1995), which are characterised by flat hard X-ray and rather steep  $\gamma$ -ray spectra (Blom et al. 1996, Tavecchio et al. 2000). Sikora et al. (2002) proposed that the prominent IC bump seen in this type of blazars can be explained by ERC dominated by the interactions of relativistic electrons with the near-IR photons from a hot dusty torus. Our SED modelling of the previous section confirms this scenario also in the case of PKS 1830–211 SSC emission is indeed found not enough efficient to reproduce the IC bump and the ERC emission on optical-UV photons from the BLR gives too much energetic  $\gamma$  rays.

A complete understanding of the emission properties of PKS 1830–211, however, presents some difficulties arising from the presence of the gravitational lens. Radio, optical and X-ray data do not give a consistent picture on the absorption of the two lensed components. The large brightness difference observed by Courbin et al. (2002) in *HST* images was explained by a differential extinction  $\Delta A_V \simeq 8.5$ . One can expect that X-ray images at energies lower than 2 keV would show a SW component much weaker than the NE, however this effect is not observed in our data (see Section 2). Spatially resolved high resolution radio spectroscopy of HCO and HCN transitions at the lens redshift (Swift et al. 2001) showed that there is no absorption in the NE image, while the SW one presents optically thick absorption with a complex structure. Molecular clouds on the radiation path of the

SW component can be then responsible of the differential absorption, however the dust to gas density ratio should be lower than the mean galactic value to account for the much higher optical extinction.

The spectral behaviour of PKS 1830–211 at low X-ray energies is characterized by strong absorption. In Figure 3 we show the spectrum, in the rest frame, of the combined *Chandra* observations as the ratio data to model assuming a power-law absorbed by Galactic gas. The ratio is not effected by instrumental response and Galactic absorption. We found that the spectrum below 5-6 keV (source frame) flattens indicating absorption in excess of the Galactic one, probably due to the lens galaxy at  $z=0.89$  and with a column density  $N_H \sim 10^{22} \text{ cm}^{-2}$ . However a remarkably similar shape is shown in Figure 5 of Yuan et al. (2003) in the case of the *XMM-Newton* observations of RX J1028.6–0844 ( $z=4.276$ ), GB1428+4217 ( $z=4.72$ ) and PMN J0525–3343 ( $z=4.4$ ). The energy of the break is similar in all sources, with a power-law photon index  $\Gamma \simeq 1$ . This evidence strongly encourage a common scenario in all these high redshift sources where absorption plays a role. The most plausible hypothesis (Fabian et al. 2001) includes the presence of a warm gas in the nuclear region (similar to that observed in Sy 1 galaxies). This warm gas is intrinsic to the source and is characterized by a column density  $N_{H,z} \sim 10^{23} \text{ cm}^{-2}$ . In the case of PKS 1830–211 this model seems to be supported by a marginal evidence of an emission line at the observed energy 2.15 keV, that can be interpreted as a blueshifted iron line ( $v/c \simeq 0.18$ ).

Further *Chandra* and *XMM-Newton* observations will help to understand the nature of the absorption in PKS 1830–211 and in the other radio-loud quasars at high redshift.

*Acknowledgements.* ADR would like to thank A. Bazzano and P. Ubertini for useful discussions. We acknowledge financial support by ASI (Italian Space Agency) via contract I/R/041/02. Part of this work was performed with the financial support Università La Sapienza di Roma.

## References

- Bassani L., Malizia A., Stephen J.B. et al. 2004, Proc. “V INTEGRAL Workshop”, Munich February 2004, ESA SP-552, astro-ph/040442
- Bird A.J., Barlow E.J., Bassani L. et al. 2004, ApJ, 607, L33
- Blazewski M., Siemiginowska A., Sikora M., Moderski R., Bechtold J. 2004, ApJ 600, L27
- Bloemen H., Bennet K., Blom J.J. et al. 1995, A&A 293, L1
- Blom J.J., Bennet K., Bloemen H. et al. 1996, A&AS 120, 507
- Celotti A. & Fabian A.C., 1993, MNRAS 264, 128
- Courbin F., Meylan G., Kneib J.P., Lidman C. 2002, ApJ 575, 95
- Fabian A.C., Celotti A., Iwasawa K. et al. 2001, MNRAS 323, 373
- Fiore F., Elvis M., Giommi P., Padovani P. 1998, ApJ 492, 79
- Goldwurm A., David P., Foschini L. et al. 2003, A&A 411, L223
- Hartman R. C., Bertsch D.L., Bloom S. D. et al. 1999, ApJS 123, 79
- Hartman R. C., Böttcher M., Aldering G. et al. 2001, ApJ 553, 683
- Lidman C., Courbin F., Meylan G. et al. 1999, ApJ 514, L57
- Lovell J.E., Jauncey D., Reynolds J.E. et al. 1998, ApJ 508, L51
- Mathur S. & Nair S., 1997, ApJ 484, 140
- Mattox J.R., Schachter J., Molnar L., Hartman R.C., Patnaik A.R. 1997, ApJ 481, 95
- Nair S., Narashima D., Pramesh Rao A., 1993, ApJ 407, 46
- Oshima T., Mitsuda K., Ota, N. et al. 2001, ApJ 551, 929
- Pramesh Rao A. & Subrahmanyam R. 1988, MNRAS 231, 229
- Revnivtsev M.G., Sunyaev R.A., Varshalovich D.A. et al. 2004, Astro. Lett., 30, 382
- Reeves J.N., Turner M.J.L., 2000, MNRAS 316, 234
- Shakura N.I., Sunyaev R.A., 1973, A&A 24, 337
- Schlegel D.J., Finkbeiner D.P., Davis M., 1998, ApJ 500, 525
- Sikora M., Madjeski G., Moderski R., Poutanen J. 1997, ApJ 484, 108
- Sikora M., Blazewski M., 2002, ApJ 577, 78
- Stark A.A., Gammie C.F., Wilson R.W. et al. 1992, ApJS, 79, 77
- Swift J.J., Welch W.J., Frye B.L., 2001, ApJ 548, L29
- Terrier R., Lebrun F., Bazzano, A. 2003, A&A, 411, L167
- Tavecchio F., Maraschi L., Ghisellini G. et al. 2000, ApJ 543, 535
- Wiklund T., Combes F., 1996, Nature 379, 139
- Winn J.M., Kochanek C.S., McLeod B.A. et al. 2002, ApJ 575, 103
- Worsley M.A., Fabian A.C., Turner A.K., Celotti A., Iwasawa K. 2004, MNRAS 350, 207
- Yuan W., Fabian A.C., Celotti, A., Jonker, P.G. 2003, MNRAS 346, L7